Uncertainty quantification in gear remaining useful life prediction through an integrated prognostics method

Fuqiong Zhao, Zhigang Tian*, Yong Zeng

Key Words - Gear, Remaining useful life, Prediction, Integrated prognostics, Finite element modeling, Bayesian updating, vibration

Abstract - Accurate health prognosis is critical for ensuring equipment reliability and reducing the overall life-cycle costs. The existing gear prognosis methods are primarily either model-based or data-driven. In this paper, an integrated prognostics method is developed for gear remaining life prediction, which utilizes both gear physical models and real-time condition monitoring data. The general prognosis framework for gears is proposed. The developed physical models include a gear finite element (FE) model for gear stress analysis, a gear dynamics model for dynamic load calculation, and a damage propagation model described using Paris' law. A gear mesh stiffness computation method is developed based on the gear system potential energy, which results in more realistic curved crack propagation paths. Material uncertainty and model uncertainty are considered to account for the differences among different specific units that affect the damage propagation path. A Bayesian method is used to fuse the collected condition monitoring data to update the distributions of the uncertainty factors for the current specific unit

* F. Zhao is with Department of Mechanical and Industrial Engineering, Concordia University. 1515 Ste-Catherine Street West EV-S2.314, Montreal, QC H3G 2W1, Canada (e-mail: fqzhao1983@hotmail.com).

Z. Tian is with Concordia Institute for Information Systems Engineering, Concordia University. 1515 Ste-Catherine Street West EV-7.637, Montreal, QC H3G 2W1, Canada (e-mail: tian@ciise.concordia.ca).

Y. Zeng is with Concordia Institute for Information Systems Engineering, Concordia University. 1515 Ste-Catherine Street West EV-7.633, Montreal, QC H3G 2W1, Canada (e-mail: yong.zeng@concordia.ca).

being monitored, and to achieve the updated remaining useful life prediction. An example is used to demonstrate the effectiveness of the proposed method.

Notation List

a	crack length
m, C	material parameters in Paris' law
N	loading cycles
ΔK	stress intensity factor range
K_I	mode I stress intensity factor
K_{II}	mode II stress intensity factor
L	edge length of triangular singular element
E	Young's modulus
ν	Poisson's ratio
u	nodal displacement in x direction
v	nodal displacement in y direction
θ	crack extension angle
r	ratio of mode I and mode II stress intensity factors
F	dynamic tooth load
F_a	horizontal force component
F_b	vertical force component
k_t	total mesh stiffness
k_h	Hertzian mesh stiffness
k_b	bending mesh stiffness
k_s	shear mesh stiffness
k_a	axial compressive mesh stiffness
Δa	crack length increment
W	pinion tooth width

α_1	force decomposition angle
α_2	half of base tooth angle
G	shear modulus
I_x	area moment of inertia of the section
A_x	area of section
ε	model uncertainty
e	measurement error
τ	standard deviation of measurement error
a_C	critical crack length
ΔN	incremental number of loading cycles
$\lambda\Delta N$	inspection interval
H	training set
R	test set
$f_{prior}(m)$	prior distribution of m
$l(a\|m)$	likelihood function in Bayesian inference
$f_{post}(m\|a)$	posterior distribution of m
$\mathcal{P}$	set of degradation paths

Abbreviations:

CBM: condition based maintenance
PHM: prognostics and health management
ANN: artificial neural network
RUL: remaining useful life
SIF: stress intensity factor
FE: finite element
HPSTC: highest point of single tooth contact

1. Introduction

Accurate health prognosis is critical for ensuring equipment reliability and reducing the overall life-cycle costs, by taking full advantage of the useful life of the equipment. Prognostics is a critical part in the framework of condition based maintenance (CBM) or prognostics and health management (PHM) [1-2]. Condition monitoring data, such as vibration, acoustic emission, imaging and oil analysis data can be collected and utilized for equipment health monitoring and prediction. Gearbox is a basic component in machine systems, and it is used to transmit power and to change the velocity. Gears may suffer from various degradation and failure modes, such as crack, surface wear and corrosion, while crack at the gear tooth root is the most important failure mode [3], which is initiated due to repetitive stress. We focus on crack at the gear tooth root in this study.

Existing gear prognosis methods can be roughly classified into model-based (or physics-based) methods and data-driven methods [1-2]. The model-based methods predict the equipment health condition using component physical models, such as finite element (FE) models and damage propagation models based on damage mechanics, and generally do not use condition monitoring data in an integrated way [2]. Some model-based methods also require data to estimate the current damage status of the monitored component or system, but the condition monitoring data does not affect the physical model parameters, such as materials parameters. Li and Lee [4] proposed a gear prognosis approach based on FE modeling where the condition monitoring data is used to estimate the current crack length. Noticing the periodicity of the meshing stiffness, an embedded model was proposed to estimate the Fourier coefficients of the meshing stiffness expansion. Besides, the software DANST was used to calculate the dynamic load on cracked tooth at different crack lengths. The damage propagation model based on Paris' law was used to predict crack propagation. Kacprzynski et al. [5] presented a gear prognosis tool using 3D gear FE modeling and considered various uncertainty factors in damage propagation, while the condition monitoring information is used to estimate the current crack length with uncertainty. Tian et al. [3] used gear dynamic simulation model and advanced signal processing tools for gear damage assessment. Marble et al. [6] developed a method for health condition prediction of propulsion system bearings based on a bearing spall propagation physical model and a FE model. For complex equipments, there are significant challenges in building authentic

physics-based models for describing the equipment dynamic response and damage propagation processes.

Data-driven methods do not rely on physics based models, and only utilize the collected condition monitoring data for health prediction. The data-driven methods achieve health prognosis by modeling the relationship between equipment age, condition monitoring data, and equipment degradation and failure time, and training based on historical data is critical. Jardine et al developed the Proportional Hazards Model based methods for equipment prognosis and CBM [1, 7]. Artificial neural network based methods have been developed by Gebraeel et al. [8-9], Lee et al. [10], Tian et al. [11], etc. Tian and Zuo [12] presented a gear health condition prediction approach using recurrent neural networks. Bayesian updating methods have been investigated in equipment prognostics for utilizing the real-time condition monitoring data [13-14]. Data driven methods cannot take advantage of the degradation mechanism information in the physical models, and they are generally not very effective if sufficient data is not available.

Integrated prognostics methods (or hybrid methods) have also been reported mainly in the field of health monitoring and prognosis for structures [27]. Integrated methods aim at fusing physical models and condition monitoring data, where condition monitoring data are used not just to estimate the current damage size, but mainly to update physical model parameters such as materials parameters c and m in the Paris' Law. The particle filter based framework was developed by Orchard and Vachtsevanos [28-29] for the for failure prognosis of planetary carrier plate. Bayesian inference has been used to update model parameters based on condition monitoring data in several studies [15, 30].

In this paper, an integrated gear prognosis method is developed by utilizing both gear physical models and real-time condition monitoring data in an integrated way. The physical models include the FE model for gear stress analysis, the gear dynamics model for dynamic load calculation and the damage propagation model described using Paris' law. Different units of the same type can have different failure times, and the internal reason behind it is that there are uncertainties such as materials uncertainty and model uncertainty. Thus, the objective of the integrated prognosis is to identify the distributions of the material and model uncertainties for the current specific unit being monitored by fusing the condition monitoring data. Such ideas have been investigated in damage propagation of structures [15], but the issue has not been studied for gears, which are rotating mechanical components where crack at the tooth root is the key failure

mode. To address this problem, we need to particularly develop the general integrated prognosis framework for gears, the FE model, and the method for fusing the condition monitoring data to update the model and to achieve the updated remaining useful life prediction. These are key contributions of this paper.

For crack propagation computation in the gear physical models, the gear mesh stiffness is required. Tian et.al [25] developed a method based on the potential energy stored in the meshing gear system, considering Hertzian energy, bending energy, axial compressive energy and shear energy. However, the crack path was assumed to follow a straight line at a fixed angle with respect to the central line of tooth. In this work, we remove the assumption of straight crack path and develop a potential energy based method to calculate the mesh stiffness, which results in a more realistic curved crack propagation path. This is another key contribution of this work.

The remainder of this paper is organized as follows. The gear physical models are presented in Section 2. The proposed integrated gear prognosis method is discussed in details in Section 3. Section 4 presents examples to demonstrate the procedure and effectiveness of the proposed prognosis approach. Conclusions are given in Section 5.

2. Physical models of gears with crack

Two types of physical models are used in this work for gear prognostics: a FE model and a damage propagation model. The FE model is used to analyze the stress particularly at gear tooth root. The damage propagation model, which is described using Paris' law, is for describing the crack propagation over time.

2.1 Finite element modeling for gear

FE model is widely used for stress and strain analysis for solid structure and machine components when the domains of variables and loading condition are too complex to obtain an analytical solution. The FE models are built in various ways in the literature and related software packages provide an easy way for numerical simulation. The software, FRANC2D, was used for investigation of gear crack propagation problem in many publications because of its unique

feature, the capability of extending crack automatically [4-5]. Kacprzynski et al. [5] built a 3D FE model to analyze the crack propagation in gears.

In this study, we consider spur gear which is a type of symmetric gear and for which the load in the gear face width is uniformly distributed. A 2D FE model is thus selected for less computation work. The software FRANC2D is used for building the gear FE model and for stress analysis. Initial crack is inserted at the position with the maximum bending stress, perpendicular to the profile. Then the crack will be propagated in the direction determined by the stress intensity factor (SIF). The applied loads on the tooth at different crack lengths are obtained by solving the dynamics equations of gear system. Plane strain condition is assumed. More details of the FE model used in this work will be given later in this paper.

2.2 The damage propagation model

The damage propagation model used in this study is for describing crack propagation in gear tooth over time. Most of the existing models are based on empirical Paris' law [16], which identifies the relationship between crack growth rate and stress state. Apart from the range of SIF, Collipriest model [17] took three other factors into account, the effect of load ratio, instability near toughness property and stress intensity threshold factor. In order to deal with hardness of tooth layers, Inoue model [18] treated all the parameters as functions of hardness distribution. Experimental results of fatigue crack tests have shown that the crack propagation have three distinct regions. Paris' law applies to the stable region where log-log plots of $\frac{da}{dN}$ versus ΔK is linear.

In this paper, the basic Paris' law is selected as damage propagation model given by

$$\frac{da}{dN} = C(\Delta K)^m, \tag{1}$$

where $\frac{da}{dN}$ is crack growth rate, ΔK is the range of SIF, C and m are material dependent constants which are generally experimentally estimated by fitting fatigue test data. Due to variations in manufacturing and testing process as well as human factors, uncertainties exist in these parameters. These uncertainties are major causes of quite different failure times for different units of the same type of gear, even if they are used in the same environment. However, the material parameter of a specific gear unit may have a very narrow distribution or even

deterministic value. Once the distributions of the parameters for the specific unit are determined, much more accurate prediction can be obtained for the failure time. For the unit being monitored, the condition monitoring data is the unit-specific information that can be utilized to determine and update the parameter distributions for the specific unit. In this study, Bayesian inference will be used to update material parameter distributions every time crack length estimation is available through condition monitoring data.

3. The Proposed Integrated Prognostics Method for Gears

An integrated prognostics method is proposed in this paper, whose framework is shown in Fig. 1. There are basically two parts separated by a dashed line in the figure: the model based part on the left hand side, and the data-driven part on the right hand side. In the model-based part, the dynamic model of the gear system is used to determine the dynamic load. The crack at gear root will affect mesh stiffness greatly, and thus the dynamic load on that cracked tooth. It is necessary to account for the load change due to crack increase since the loading condition affects stress intensity factor to a large degree. Hence, a gear dynamic model is applied to calculate the dynamic load on gear tooth at different crack length. The calculated dynamic load is used in the gear FE model, and the output is the SIF at the crack tip. SIF as a function of crack length and loading is used in the crack propagation model, which is described by Paris' law. With the current crack length, the failure time and the remaining useful life (RUL) distributions can be predicted by propagating the uncertainties in the materials parameters through the degradation model. In the data-driven part, crack evaluation model is used to estimate the crack length (with uncertainty) based on condition monitoring data. The current measured crack length can be used to update the distributions of the uncertainty factors, i.e., the materials parameters M and C and the model uncertainty, and thus to achieve more accurate RUL prediction based on the refined parameter and condition estimations for the specific unit. The Bayesian inference will be used in this work for this purpose. Details of the different parts of the approach will be discussed in the following subsections.

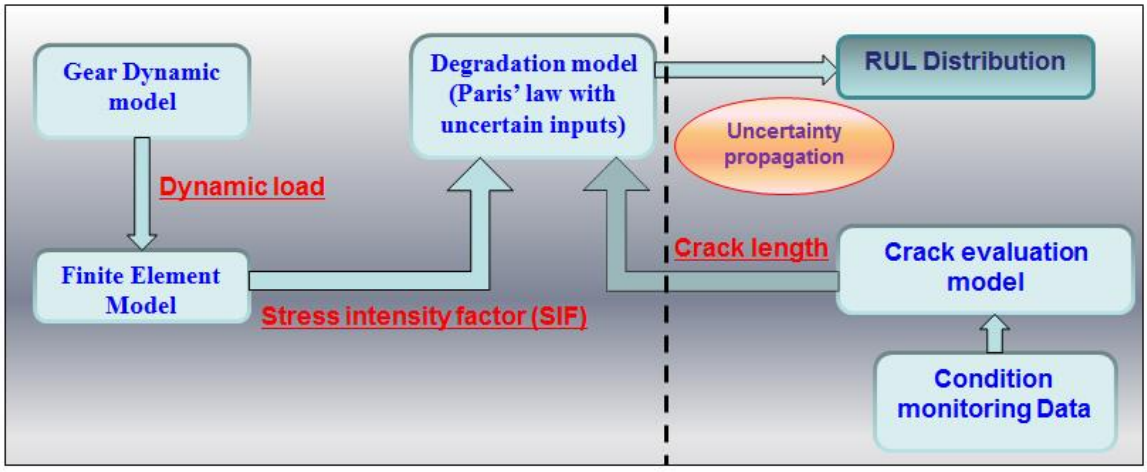

Fig. 1. Framework of the proposed integrated prognostic approach

3.1 Gear stress analysis using FE model

FE model described in Section 2.1 is used to calculate the stress intensity factor at crack tip, which is a key variable used in quantifying the gear crack propagation. The stress analysis is under the principle of linear elastic fracture mechanics theory. The method to calculate stress intensity factor is termed as displacement correlation method, which employs singular element to model stress singularity near crack tip. The said singular element is a type of finite element modified by positioning the point at quarter of element edge instead of middle point. It enables such element to exhibit $\frac{1}{\sqrt{r}}$ singularity along element edge and greatly improves accuracy and reduces the need for a high degree of mesh refinement at crack tip. The 6 nodes triangular singular element around the crack tip are shown in Fig. 2.

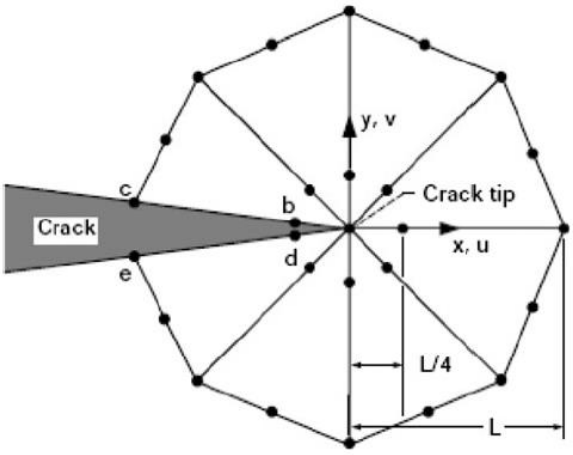

Fig. 2. Singular element [19]

The displacement correlation method can be used to calculate the stress intensity factor using nodal displacements, as shown in the following formulas:

$$K_I = \frac{E}{2(1+\nu)(\kappa+1)}\sqrt{\frac{2\pi}{L}}[4(v_b - v_d) + v_e - v_c] \tag{2}$$

$$K_{II} = \frac{E}{2(1+\nu)(\kappa+1)}\sqrt{\frac{2\pi}{L}}[4(u_b - u_d) + u_e - u_c] \tag{3}$$

where K_I and K_{II} are two types of SIF corresponding to two modes of crack. L is element edge length, E is Young's modulus, ν is Poisson's ratio, u and v are nodal displacements and

$$\kappa = \begin{cases} 3 - 4\nu & \text{(plane strain)} \\ \dfrac{3-\nu}{1+\nu} & \text{(plane stress).} \end{cases} \tag{4}$$

The published results show that in crack propagation, K_I is dominating over K_{II} [20]. Hence, in Paris' law for crack propagation shown in Eq. (1), only the range of K_I is used.

3.2 Gear dynamics model

Most of the studies on the gear crack propagation problem considered constant static load on the meshing teeth. They investigated how the crack propagates under a fixed force on the tooth.

Their main work was to use the fracture model to analyze the stress and strain near the crack tip to determine the crack growth rate as well as the growth direction. Then the crack propagation model was used to estimate the life cycles until failure. Therefore, the entire crack path and the service life of the gear can be obtained. However, the appearance of crack would reduce the stiffness of the tooth so that the load on the tooth will be affected by this reduction. The purpose of the gear dynamics model in this paper is similar to that in [4], which is to calculate the dynamic load on cracked tooth at different crack lengths. At each crack length, the maximum dynamic load is selected to be applied on the cracked tooth to drive the crack extension.

3.2.1 Dynamic load

As mentioned above, dynamic load on cracked tooth will change due to mesh stiffness change affected by crack occurrence. To calculate the dynamic load values at different crack length, a gear dynamic model with 6 degree-of-freedom is used in this paper. This mathematical model with torsional and lateral vibration was reported by Bartelmus [21]. We assume that all gears are perfectly mounted rigid bodies with ideal geometries. Inter-tooth friction is ignored here for simplicity. The governing motion equations are

$$m_1\ddot{y}_1 = F_k + F_c - F_u - F_{uc} \tag{5}$$

$$m_2\ddot{y}_2 = F_k + F_c - F_l - F_{lc} \tag{6}$$

$$I_1\ddot{\theta}_1 = M_{pk} + M_{pc} - R_{b1}(F_k + F_c) \tag{7}$$

$$I_2\ddot{\theta}_2 = R_{b2}(F_k + F_c) - M_{gk} + M_{gc} \tag{8}$$

$$I_m\ddot{\theta}_m = M_1 - M_{pk} + M_{pc} \tag{9}$$

$$I_b\ddot{\theta}_b = -M_2 - M_{pk} + M_{pc} \tag{10}$$

$$F_k = k_t(R_{b1}\theta_1 - R_{b2}\theta_2 - y_1 + y_2) \tag{11}$$

$$F_c = c_t\left(R_{b1}\dot{\theta}_1 - R_{b2}\dot{\theta}_2 - y_1 + y_2\right) \tag{12}$$

$$F_u = k_1 y_1 \tag{13}$$

$$F_{uc} = c_1\dot{y}_1 \tag{14}$$

$$F_l = k_2 y_2 \tag{15}$$

$$F_{lc} = c_2\dot{y}_2 \tag{16}$$

$$M_{pk} = k_p(\theta_m - \theta_1) \tag{17}$$

$$M_{pc} = c_p\left(\dot{\theta_m} - \dot{\theta_1}\right) \tag{18}$$

$$M_{gk} = k_g(\theta_2 - \theta_b) \tag{19}$$

$$M_{gc} = c_g\left(\dot{\theta_2} - \dot{\theta_b}\right) \tag{20}$$

The assumptions and the parameter values for this system are adopted from [3] except for values of input motor torque and output load torque, because large load is needed to drive the crack to propagate quickly in failure test. The system is solved using Matlab's ODE15s function.

Let δ represent the backlash. The dynamic tooth load F is calculated based on the formulas given by Lin et al. [22]. Here, the lateral displacements are added.

Case (i) $R_{b1}\theta_1 - R_{b2}\theta_2 - y_1 + y_2 > 0$, which is the normal operating case:

$$F = k_t(R_{b1}\theta_1 - R_{b2}\theta_2 - y_1 + y_2) + c_t\left(R_{b1}\dot{\theta}_1 - R_{b2}\dot{\theta}_2 - \dot{y}_1 + \dot{y}_2\right) \tag{21}$$

Case (ii) $R_{b1}\theta_1 - R_{b2}\theta_2 - y_1 + y_2 \leq 0$ and $|R_{b1}\theta_1 - R_{b2}\,\theta_2 - y_1 + y_2| \leq \delta$, where the gear pair will separate:

$$F = 0 \tag{22}$$

Case (iii) $R_{b1}\theta_1 - R_{b2}\theta_2 - y_1 + y_2 < 0$ and $|R_{b1}\theta_1 - R_{b2}\,\theta_2 - y_1 + y_2| > \delta$, where the gears will collide backside:

$$F = k_t(R_{b2}\theta_2 - R_{b1}\theta_1 - y_2 + y_1) + c_t\left(R_{b2}\dot{\theta}_2 - R_{b1}\dot{\theta}_1 - \dot{y}_2 + \dot{y}_1\right) \tag{23}$$

The dynamic load on tooth at contact point is the sum of stiffness inter-tooth force $k_t(R_{b1}\theta_1 - R_{b2}\theta_2 - y_1 + y_2)$ and damping inter-tooth force $c_t(R_{b1}\dot{\theta}_1 - R_{b2}\dot{\theta}_2 - \dot{y}_1 + \dot{y}_2)$. Here k_t is the meshing stiffness at contact point and c_t is the mesh damping coefficient. Since both the torsional and lateral vibration are considered in this dynamic model, the effect of lateral vibration on relative gear tooth displacements as well as on velocities should be taken into account. In this study, the dynamic load F in case (iii) is considered to be zero for simplicity.

A crack in pinion root is inserted at the second tooth. Since mesh stiffness is affected directly by crack and it is the critical parameter to determine the dynamic load, the mesh stiffness for the cracked tooth in pinion during its meshing is calculated first.

3.2.2 Total mesh stiffness calculation

Yang and Lin [24] proposed a method which used the potential energy stored in the meshing gear system to calculate the mesh stiffness between the meshing teeth. The energy includes Hertzian energy, bending energy and axial compressive energy. Tian et.al [25] improved this energy method by adding shear energy as well which affects the total mesh stiffness greatly. Meanwhile, the calculation of mesh stiffness using potential energy method for the gear with crack was given. The crack path was assumed to be straight at a fixed angle with respect to the central line of tooth. Furthermore, in [3, 26], the crack path was extended based on [25], say, when the crack reached to the central line, it would change the direction which was assumed to be exactly symmetric around the tooth's central line so that the whole crack path could go through the entire tooth. However, according to the experimental results, the crack propagates in a curved line instead of a straight line due to the stress concentration at the tooth roots. The crack propagation direction should be determined by the stress status near the crack tip. To be more precise, under the principle of linear elastic mechanics theory, the two-dimensional crack extension angle is computed by the ratio of mode I and mode II stress intensity factor $r = \frac{K_I}{K_{II}}$,

$$\theta = 2\arctan\left(\frac{r \pm \sqrt{r^2+8}}{4}\right). \tag{24}$$

In this paper, based on the method proposed in [25, 26], we remove the assumption of straight crack path and develop a potential energy method to calculate the mesh stiffness of meshing gear pair, of which one tooth can have a curved crack propagation path. This "curved" crack propagation path is formed by connecting a series of straight crack increments. Different from the straight crack assumption, the intersection angle, β, between the vertical line passing crack tip and the line connecting tooth root to crack tip varies. The meshing gear system in this study has a contact ratio between 1 and 2, thus at certain given time, there exist two meshing situations: single pair contact and double pair contact. For these two types of contact duration, the total effective mesh stiffness can be expressed respectively as [25]:

$$k_t = \frac{1}{1/k_h+1/k_{b1}+1/k_{s1}+1/k_{a1}+1/k_{b2}+1/k_{s2}+1/k_{a2}} \quad \text{(single pair contact)} \tag{25}$$

$$k_t = \sum_{j=1}^{2} \frac{1}{1/k_{h,j}+1/k_{b1,j}+1/k_{s1,j}+1/k_{a1,j}+1/k_{b2,j}+1/k_{s2,j}+1/k_{a2,j}} \quad \text{(double pair contact)} \tag{26}$$

where k_h, k_b, k_s, k_a represent the Hertzian, bending, shear and axial compressive mesh stiffness respectively. Besides, $j = 1$ represents the first pair of meshing teeth and $j = 2$ represents the

second pair. One crack is inserted at the pinion tooth root with initial length of a_0, The procedure to calculate the tooth stiffness with a curved crack path is given as follows.

As shown in Fig. 3, the crack increment at each crack extension step is set to Δa. The crack tip is denoted by T_i, where the index i represents the crack propagation step. The crack length grows by Δa in the direction determined by (24). Because the associated formulas to compute cracked tooth stiffness are related to four different cases, depending on the teeth meshing contact point and the crack tip position as well, in Fig. 3, the index of $i = 1, 2, 3, 4$ only symbolizes the four mentioned typical cases, and it does not mean that there are only these four crack tips. According to [25], the Hertzian and axial compressive stiffness are not affected by crack occurrence while the bending stiffness and shearing stiffness will change after the crack is introduced.

The base circle of pinion centers at O with the radius of R_{b1}. The contact point C are travelling along the tooth profile $\widetilde{SM}$ and the angle of $\alpha_1$is determined by the tangential line passing C. Since the force F is applied at the contact point C, perpendicular to the tangential line, the angle α_1 also serves as the force decomposition angle to the horizontal direction $F_b = F\cos\alpha_1$ and vertical direction $F_a = F\sin\alpha_1$. Additionally, the points G_i represent the intersection points between the vertical line passing crack tip and the tooth profile. And Z_i are the pedals on base circle of tangential line passing G_i. Accordingly, g_i is the distance from G_i to the tooth root S and α_{gi} is the angle between G_iZ_i and OZ_i. If the crack tip passes the central line, denote the symmetric point regarding to central line OP of G_i as G_i', and the associated α_{gi} is defined as the angle between $G_i'Z_i$ and OZ_i. Lastly, α_2 represents the half of the base tooth angle.

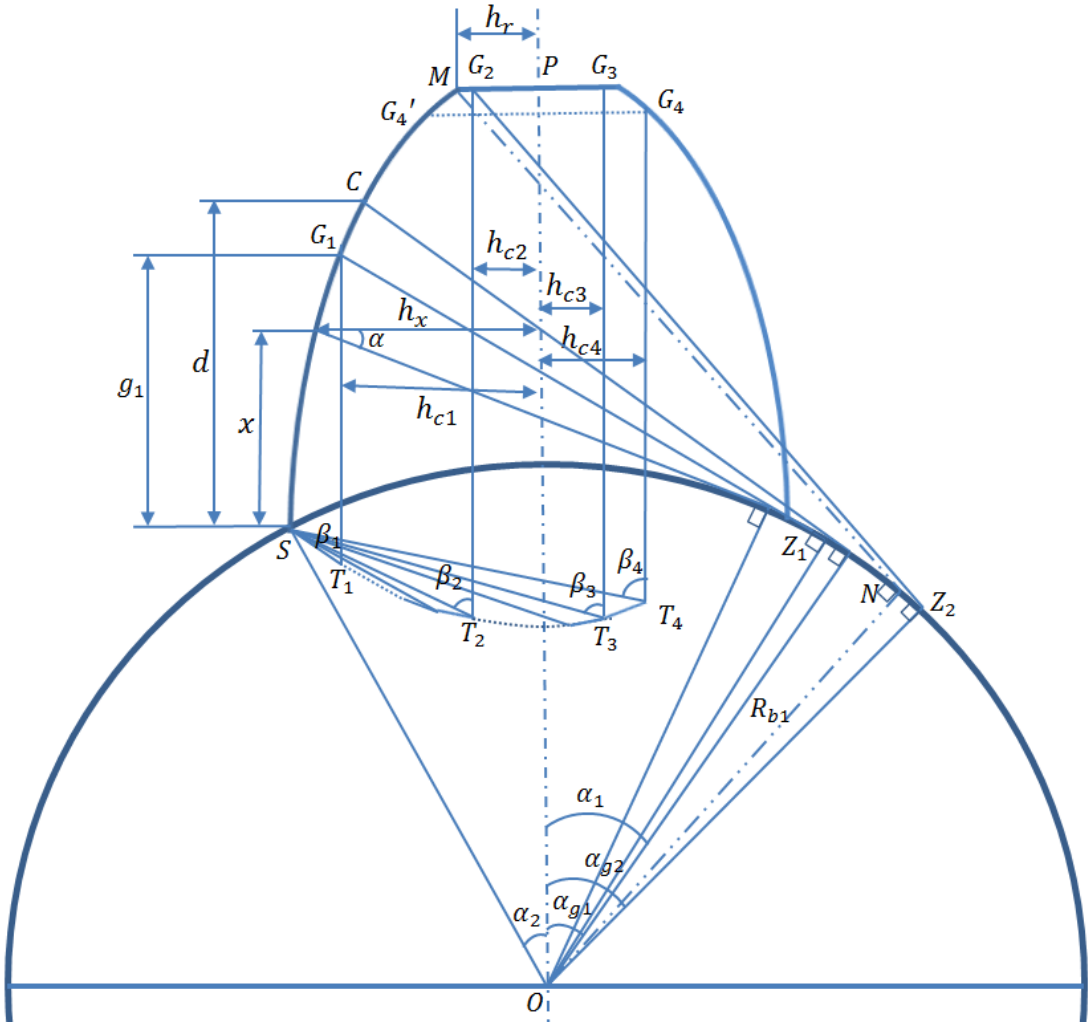

Fig. 3 Cracked tooth model

Based on the results in [25], the Hertzian stiffness, independent of the contact position, is given by

$$k_h = \frac{\pi EW}{4(1-\nu^2)} \tag{27}$$

where E is Young's modulus, W is tooth width and ν is the Poisson's ratio. And the axial compressive stiffness is

$$\frac{1}{k_a} = \int_{-\alpha_1}^{\alpha_2} \frac{(\alpha_2-\alpha)\cos\alpha\sin^2\alpha_1}{2EL[\sin\alpha+(\alpha_2-\alpha)\cos\alpha]}\mathrm{d}\alpha\ . \tag{28}$$

The bending energy stored in a meshing gear tooth, based on beam theory, can be obtained by

$$U_b = \int_0^d \frac{M^2}{2EI_x}\mathrm{d}x = \int_0^d \frac{[F_b(d-x)-F_a h]^2}{2EI_x}\mathrm{d}x \ , \tag{29}$$

and the shear energy is given by

$$U_s = \int_0^d \frac{1.2{F_b}^2}{2GA_x}\mathrm{d}x \tag{30}$$

$$G = \frac{E}{2(1+\nu)} \tag{31}$$

In the above formulas given in [24], G is shear modulus. I_x and A_x represent the area moment of inertia of the section and the area of the section, where the distance from the tooth root is x. Essentially, the calculations of I_x and A_x at different crack tip positions at different contact points determine the existence of the four mentioned circumstances to calculate tooth stiffness of cracked tooth. These four cases for stiffness calculation of cracked tooth are addressed below. Let the distance between tooth root S and G_iT_i be u_i. As said before, the purpose of index of $i = 1, 2, 3, 4$ is to indicate the four cases, not meaning there are the only four crack tip locations.

Case 1. Crack tip = T_1 (i.e., $h_{c1} \geq h_r$),

In this case,

$$I_x = \begin{cases} \frac{1}{12}(h_{c1}+h_x)^3 W, & \text{if } x \leq g_1, \\ \frac{1}{12}(2h_x)^3 W, & \text{if } x > g_1, \end{cases} \tag{32}$$

$$A_x = \begin{cases} (h_{c1}+h_x)W, & \text{if } x \leq g_1, \\ 2h_x W, & \text{if } x > g_1. \end{cases} \tag{33}$$

Case 1.1. Contact point is above G_1 (i.e., $\alpha_1 > \alpha_{g1}$) .

The bending mesh stiffness of the cracked tooth is

$$\begin{aligned} \frac{1}{k_b} = & \int_{-\alpha_{g1}}^{\alpha_2} \frac{12\{1+\cos\alpha_1[(\alpha_2-\alpha)\sin\alpha-\cos\alpha]\}^2(\alpha_2-\alpha)\cos\alpha}{EW[\sin\alpha_2 - \frac{u_1}{R_{b1}} + \sin\alpha + (\alpha_2-\alpha)\cos\alpha]^3}\mathrm{d}\alpha \\ & + \int_{-\alpha_1}^{-\alpha_{g1}} \frac{3\{1+\cos\alpha_1[(\alpha_2-\alpha)\sin\alpha-\cos\alpha]\}^2(\alpha_2-\alpha)\cos\alpha}{2EW[\sin\alpha+(\alpha_2-\alpha)\cos\alpha]^3}\mathrm{d}\alpha \end{aligned} \tag{34}$$

The shear stiffness is

$$\frac{1}{k_s}=\int_{-\alpha_{g1}}^{\alpha_2}\frac{2.4(1+\nu)(\alpha_2-\alpha)\cos\alpha\cos^2\alpha_1}{EW[\sin\alpha_2-\frac{u_1}{R_{b1}}+\sin\alpha+(\alpha_2-\alpha)\cos\alpha]}\mathrm{d}\alpha + \int_{-\alpha_1}^{-\alpha_{g1}}\frac{1.2(1+\nu)(\alpha_2-\alpha)\cos\alpha\cos^2\alpha_1}{EW[\sin\alpha+(\alpha_2-\alpha)\cos\alpha]}\mathrm{d}\alpha \tag{35}$$

Case 1.2. Contact point is below G_1 (i.e., $\alpha_1 \le \alpha_{g1}$) .

The bending stiffness and shear stiffness are given by

$$\frac{1}{k_b}=\int_{-\alpha_1}^{\alpha_2}\frac{12\{1+\cos\alpha_1[(\alpha_2-\alpha)\sin\alpha-\cos\alpha]\}^2(\alpha_2-\alpha)\cos\alpha}{EW[\sin\alpha_2-\frac{u_1}{R_{b1}}+\sin\alpha+(\alpha_2-\alpha)\cos\alpha]^3}\mathrm{d}\alpha \tag{36}$$

$$\frac{1}{k_s}=\int_{-\alpha_1}^{\alpha_2}\frac{2.4(1+\nu)(\alpha_2-\alpha)\cos\alpha\cos^2\alpha_1}{EW\left[\sin\alpha_2-\frac{u_1}{R_{b1}}+\sin\alpha+(\alpha_2-\alpha)\cos\alpha\right]}\mathrm{d}\alpha \tag{37}$$

Case 2. Crack tip = T_2 (i.e., $h_{c2} < h_r$)

In this case,

$$I_x=\tfrac{1}{12}(h_{c1}+h_x)^3W \text{ and } A_x=(h_{c2}+h_x)W \tag{38}$$

based on which, the bending stiffness and shear stiffness are obtained by

$$\frac{1}{k_b}=\int_{-\alpha_1}^{\alpha_2}\frac{12\{1+\cos\alpha_1[(\alpha_2-\alpha)\sin\alpha-\cos\alpha]\}^2(\alpha_2-\alpha)\cos\alpha}{EW[\sin\alpha_2-\frac{u_2}{R_{b1}}+\sin\alpha+(\alpha_2-\alpha)\cos\alpha]^3}\mathrm{d}\alpha$$

$$\frac{1}{k_s}=\int_{-\alpha_1}^{\alpha_2}\frac{2.4(1+\nu)(\alpha_2-\alpha)\cos\alpha\cos^2\alpha_1}{EW[\sin\alpha_2-\frac{u_2}{R_{b1}}+\sin\alpha+(\alpha_2-\alpha)\cos\alpha]}\mathrm{d}\alpha \tag{39}$$

Case 3. Crack tip = T_3 (i.e., $h_{c3} < h_r$)

In this case,

$$I_x=\tfrac{1}{12}(h_x-h_{c3})^3W \text{ and } A_x=(h_x-h_{c3})W, \tag{40}$$

the bending and shear stiffness are

$$\frac{1}{k_b} = \int_{-\alpha_1}^{\alpha_2} \frac{12\{1+\cos\alpha_1[(\alpha_2-\alpha)\sin\alpha-\cos\alpha]\}^2(\alpha_2-\alpha)\cos\alpha}{EW[-\frac{u_3}{R_{b1}}+\sin\alpha+(\alpha_2-\alpha)\cos\alpha]^3}\mathrm{d}\alpha \tag{41}$$

$$\frac{1}{k_s} = \int_{-\alpha_1}^{\alpha_2} \frac{2.4(1+\nu)(\alpha_2-\alpha)\cos\alpha\cos^2\alpha_1}{EW[-\frac{u_3}{R_{b1}}+\sin\alpha+(\alpha_2-\alpha)\cos\alpha]}\mathrm{d}\alpha \tag{42}$$

Case 4. Crack tip = T_4 (i.e., $h_{c4} \geq h_r$)

In this case,

$$I_x = \frac{1}{12}(h_x - h_{c4})^3 W \text{ and } A_x = (h_x - h_{c4})W. \tag{43}$$

Case 4.1. Contact point is above G_4' (i.e., $\alpha_1 > \alpha_{g4}$) .

$$\frac{1}{k_b} = \int_{-\alpha_{g4}}^{\alpha_2} \frac{12\{1+\cos\alpha_1[(\alpha_2-\alpha)\sin\alpha-\cos\alpha]\}^2(\alpha_2-\alpha)\cos\alpha}{EW[-\frac{u_4}{R_{b1}}+\sin\alpha+(\alpha_2-\alpha)\cos\alpha]^3}\mathrm{d}\alpha \tag{44}$$

$$\frac{1}{k_s} = \int_{-\alpha_{g4}}^{\alpha_2} \frac{2.4(1+\nu)(\alpha_2-\alpha)\cos\alpha\cos^2\alpha_1}{EW[-\frac{u_4}{R_{b1}}+\sin\alpha+(\alpha_2-\alpha)\cos\alpha]}\mathrm{d}\alpha \tag{45}$$

Case 4.2. Contact point is below G_4' (i.e., $\alpha_1 \leq \alpha_{g4}$) .

$$\frac{1}{k_b} = \int_{-\alpha_1}^{\alpha_2} \frac{12\{1+\cos\alpha_1[(\alpha_2-\alpha)\sin\alpha-\cos\alpha]\}^2(\alpha_2-\alpha)\cos\alpha}{EW[-\frac{u_4}{R_{b1}}+\sin\alpha+(\alpha_2-\alpha)\cos\alpha]^3}\mathrm{d}\alpha \tag{46}$$

$$\frac{1}{k_s} = \int_{-\alpha_1}^{\alpha_2} \frac{2.4(1+\nu)(\alpha_2-\alpha)\cos\alpha\cos^2\alpha_1}{EW[-\frac{u_4}{R_{b1}}+\sin\alpha+(\alpha_2-\alpha)\cos\alpha]}\mathrm{d}\alpha \tag{47}$$

So far we have obtained the formulas to calculate the bending stiffness and shear stiffness of cracked tooth at any crack tip position and any contact point. No matter what the crack shape is, as long as the crack tip position is identified, i.e., u_i is known, these two types of stiffness could be derived by the above formulas. Plus the Hertzian stiffness in Eq. (27) and axial compressive stiffness in Eq. (28), the total effective mesh stiffness is ready to use in the set of dynamic equations.

3.3 Uncertainty quantification in gear prognostics

The objective of integrated gear health prognostics is to predict the remaining useful life from certain moment by fusing the physical models and the condition monitoring data.

Uncertainties exist in both the model-based part and the data-driven part of the proposed integrated prognostics approach, and the uncertainties are propagated to the predicted failure time and the RUL. That is, these uncertainties are the key causes of the predicted RUL distribution. The RUL uncertainty quantification is critical when using degradation model to obtain accurate prediction results. In this section, first we define three main uncertainty sources to be accounted for, and then Paris' law is used to predict the remaining useful life at a given instant considering those uncertainties. Moreover, each time the new observation data is available, the prediction will be updated by adjusting the statistical properties of those uncertainties using Bayesian inference.

3.3.1 Modeling of uncertainty sources

In this study, three main uncertainty sources are considered when using degradation model for prediction, that is, material parameter uncertainty, model uncertainty and measurement uncertainty.

When Paris' law is applied to predict the remaining cycles until critical failure length, material parameters m and C are essential factors. The values of these two parameters are acquired by experiments in controlled environment. However, uncertainties due to variation in manufacturing, testing process, human factor and other unexpected errors still have great potential contributions to the variations in the values of m and C. In most of the research work, m and $\log C$ are assumed to follow normal distributions.

The degradation model in this paper adopts basic Paris' law as crack propagation model without considering other possible parameters which may have impact on crack propagation, such as crack closure retard, fracture toughness, load ratio etc. Therefore, an error term is introduced to represent the difference between the results obtained by Paris' law and the real observations, termed as model uncertainty and denoted by ε. Considering the model uncertainty, the modified Paris' law is written as:

$$\frac{da}{dN} = C(\Delta K)^m \, \varepsilon \tag{48}$$

In addition, measurement error e is also considered due to the errors resulting from sensor as well as crack estimation methods. In practical applications, the current crack length is generally

estimated indirectly based on the sensor data using certain damage estimation techniques, and thus there is uncertainty associated with the current crack length estimation. Here we assume measurement error, $e = a^{real} - a_{mea}$, has the following distribution,

$$e \sim N(0, \tau^2) \tag{49}$$

That is equally to say, the measured crack length, a_{mea}, obeys normal distribution centered at a^{real} with τ as the standard deviation,

$$a_{mea} \sim N(a^{real}, \tau^2) \tag{50}$$

3.3.2 Remaining useful life prediction

At a certain inspection point *t*, suppose that the measured crack length is a_t and the current loading cycle is N_t. The crack will propagate according to the Paris' law. When the critical crack length a_C is reached, the gear is considered failed. Due to the material uncertainty and model uncertainty, we will be able to obtain the predicted failure time distribution.

The Paris' law can be written as follows in Eq. (51), where ΔK denotes the range of SIF, which can be obtained using FE analysis, as a function of crack length and loading,

$$\frac{dN}{da} = \frac{1}{C(\Delta K(a))^m \varepsilon} \quad . \tag{51}$$

Let the crack increment be $\Delta a = a_{i+1} - a_i, i = t, t+1, \cdots$, then the number of remaining useful cycles experienced by the tooth from the current length a_t until it reaches critical length a_C can be calculated by discretizing Paris' law as follows:

$$\Delta N_{i+1} = N_{i+1} - N_i = \Delta a \left[C \left(\frac{\Delta K(a_{i+1}) + \Delta K(a_i)}{2} \right)^m \varepsilon \right]^{-1} \tag{52}$$

The summation $\sum(\Delta N_i), i = t, t+1, \cdots$ until critical length a_C is the total remaining cycles, or RUL. The entire failure time could be obtained by $N_t + \sum(\Delta N_i), i = t, t+1, \cdots$. Considering the uncertainties in materials properties and crack propagation model itself, there is uncertainty in the predicted RUL, as discussed before. Monte-Carlo simulation is employed to quantify the uncertainty in the predicted RUL.

3.3.3 Prediction updating using Bayesian method

Different from model-based method which only counts on the physical models or use the data to estimate the severity of the fault, the proposed integrated approach in this paper also uses condition monitoring data to adjust the model parameters. The condition monitoring data contains specific information for a specific gear under specific environment. So each time a new crack length is estimated, we have the chance to adjust the physical model parameters for the current gear being monitored and to make the RUL prediction more accurate. From one aspect, the prediction will start at a new inspection time with more accurate model parameters. From the other aspect, as we know, even though for the whole gear population there exist perhaps widely distributed material parameter values, but for a specific gear, the distribution of these parameters should be much narrower or even close to deterministic values. Therefore, the new condition monitoring data provides opportunities to reduce the uncertainty in model parameters. In this paper, Bayesian inference is used to update the distributions of the model parameters at every inspection cycle. Consider for example a simplified case where we only update the distribution of parameter m, while assuming that the other material parameter,*C*, is constant. The prior distribution for m is $f_{prior}(m)$ and the likelihood to detect the current measured crack length is $l(a|m)$. Thus, the formula to use Bayesian rule to obtain posterior distribution $f_{post}(m|a)$ is:

$$f_{post}(m|a) = \frac{l(a|m)f_{prior}(m)}{\int l(a|m)f_{prior}(m)\,dm} \tag{53}$$

At a given value of m, Paris' law is used to propagate the crack from current measured crack length to the length measured at next inspection cycle. Because of the measurement error e and model error ε, there exists a sort of likelihood to observe a crack length at next inspection cycle, i.e., to obtain the estimated crack length. Because the updating is from the one inspection cycle to the next one, we assume the crack length at the current inspection cycle is a_{curr_cycle}, incremental number of cycles is ΔN and after $\lambda\Delta N$ cycles, i.e., the inspection interval, it reaches to the length of a_{next_cycle}. Use the following discretized Paris' law to realize this extension from current inspection cycle to the next one,

$$\begin{cases} a\big((i+1)\Delta N\big) = a(i\Delta N) + (\Delta N)C\big[\Delta K\big(a(i\Delta N)\big)\big]^m \varepsilon, i = 0,1,2,\cdots,\lambda-1 \\ a(0) = a_{curr\_cycle} \end{cases} \tag{54}$$

So $a_{next\_cycle} = a(\lambda\Delta N)$. Hence considering the measurement error, the measured crack length at next inspection cycle should follow the distribution of

$$a_{mea\_next\_cycle} \sim N\left(a_{next\_cycle}, \tau^2\right) \tag{55}$$

Thus, the PDF of the normal distribution in Eq. (55) is exactly the likelihood function $l(a|m)$ in Bayesian reference. Here, the effect of model error ε on the crack length estimation mainly relies on its mean because of central limit theory. Hence, without much loss of accuracy, the likelihood function is considered to be only determined by measurement error. Let the PDF of the measured crack length at next inspection cycle, i.e., $N(a_j, \tau)$, be $g(a)$. The likelihood to observe the measured crack length of $a^*_{mea\_next\_cycle}$ is simply calculated by $g(a^*_{mea\_next\_cycle})$.

3.3.4 Prior distribution of m

Factors such as geometry, material, and errors in manufacture process can result in different values of parameter m in different gears. Therefore, a kind of statistical distribution of m for gear population exists, denoted here by N_1. However, for a specific gear being monitored, the value of m should have a very narrow distribution, denoted by N_2, or even be deterministic. This value may not be available accurately because of possible errors in experiments. Condition monitoring data of this specific gear can reflect the specific properties of this gear, which can be used to update the distribution of m from a prior in a way described in Section 3.2.3 to get more accurate RUL prediction. This section will address how to get a prior distribution of m.

First, suppose a set of degradation paths of different failed gears, $\mathcal{P}$, are available, which are collected historical data. For each degradation path corresponding to gear $i \in \mathcal{P}$, we need to estimate its material parameter m, so as to obtain the prior distribution of m based on the historical data. For path i, suppose at inspection points $INSP_j,\ j = 1, \cdots, M$, the recorded actual crack lengths are $a_j^{i\_act}, j = 1, \cdots, M$. Now we generate a simulated crack propagation history, denoted by $a^{i\_app}(m)$, corresponding to parameter m using Eq. (54), considering both model uncertainty and measurement error. At the same inspection cycles $INSP_j,\ j = 1, \cdots, M$, the simulated crack lengths are $a_j^{i\_app}(m), j = 1, \cdots, M$, respectively. Thus, the difference at the inspection point between the actual path and simulated path is: $e_j^i(m) = a_j^{i\_act} - a_j^{i\_app}(m)$. We

can find the optimal material parameter value, m_{op}^{i}, for this gear by minimizing the difference at the inspection points between the actual path and the simulated path. More specifically, the Mean-Least-Square (MLS) criteria is used, and the optimal material parameter value for path $i \in \mathcal{P}$, m_{op}^{i}, satisfies:

$$\sum_{j=1}^{M}(e_j^i(m_{op}^i))^2 \leq \sum_{j=1}^{M}(e_j^i(m))^2, \qquad \forall m \tag{56}$$

Lastly, by fitting the optimal material parameter values for all failed gears using normal distribution, we can obtain the mean μ_{prior}^{m} and the standard deviation σ_{prior}^{m} for the prior distribution of m. Thus, the PDF of prior distribution of m is

$$f_{prior}(m) \sim N\left(\mu_{prior}^{m}, \left(\sigma_{prior}^{m}\right)^2\right) \tag{57}$$

After obtaining $f_{prior}(m)$, the approach stated in Section 3.3.3 can be implemented to update the distribution of parameter m for the gear being monitored using Bayesian inference once condition monitoring data is available.

4. Example

In this section, a numerical example of gear life prediction using the proposed integrated prognostics approach is presented. Simulated crack propagation data, i.e., the degradation paths, are generated and used by considering the various uncertainty factors in real gear systems. The generated degradation paths are divided into two sets: the training set is used to obtain the prior distribution for parameter m, and the test set is used to test the prediction performance of the proposed prognostics approach. The training set can be considered to be the available historical gear degradation histories.

4.1 Introduction

In this example, a 2D finite element model of single cracked tooth is built in software of FRANC2D. This software has its unique feature to analyze crack propagation problem. The singular mesh near crack tip will be generated automatically, and based on the stress analysis, the crack will be propagated and the associated stress intensity factors at each crack length will be

recorded accordingly. The material and geometry properties of this specific spur gear used in this example are listed in Table 1. Suppose the critical crack length is $a_c = 5.2$mm, which is 80% of the full length. Beyond this failure threshold, the crack will propagate very fast and the tooth breakoff is imminent. The FE model is shown in Fig. 4.

The gear dynamic system mentioned in Section 3.2 is used to calculate the dynamic load on this cracked tooth. To drive the crack to propagate, large torque is selected. The input torque is selected as 320Nm and output load torque is 640Nm. Besides the torques, other values for the parameters in dynamic system are exactly the same as those in paper [3]. The rotation speed of gearbox is 30Hz. The mesh stiffness of the first two teeth on the pinion for the healthy tooth is shown in Fig. 5. The crack is introduced at the root of the second tooth on pinion and the crack growth will end until it reaches the critical length which is 5.2mm. The mesh stiffness at the critical length is shown in Fig. 6. In these two figures, the blue solid line represents the total mesh stiffness and the mauve dash line represents the mesh stiffness of the gear pair having the cracked tooth. From these figures we can see that the mesh stiffness is greatly reduced due to crack.

With the mesh stiffness at different crack length available, MATLAB ODE15s function is then used to solve the dynamic equations (5−20). Dynamic loads at every contact points, i.e., at every rotation angle, can then be calculated using Eq. (22-23). For demonstration, Fig. 7 shows the dynamic load and static load on the cracked tooth with the crack length of 3.5mm when it meshes. The maximum dynamic load appears at the rotation angle of 13.89 degree, higher than the static load. The results show that for the entire crack path, the position of maximum dynamic load will move forward a little bit as the crack length increases but the movement is less than 1 degree so that the load is considered being applied at a fixed position which corresponds to the rotation angle of around 14 degree.

Table 1. Material properties and main geometry parameters.

Young's modulus (Pa)	Poisson's ratio	Module (mm)	Diametral pitch (in^{-1})	Base circle radius (mm)	Outer circle (mm)	Pressure angle (degree)	Teeth No.
2.068e11	0.3	3.2	8	28.34	33.3	20	19

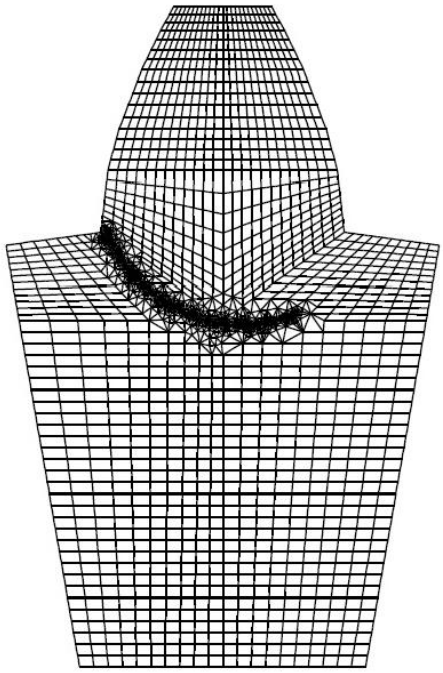

Fig. 4. 2D FE model for spur gear tooth

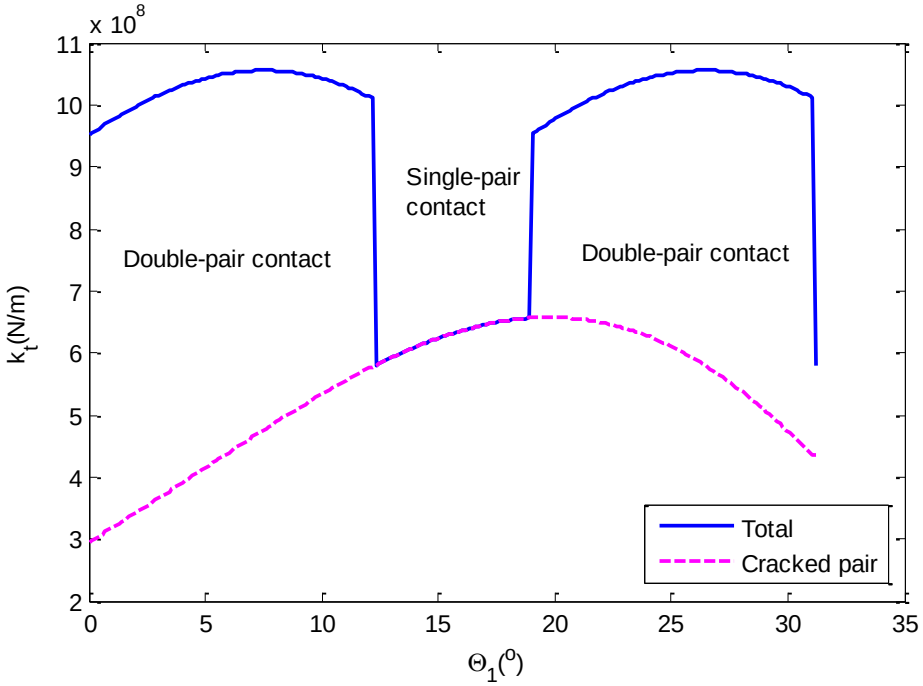

Fig. 5. Mesh stiffness of healthy gears

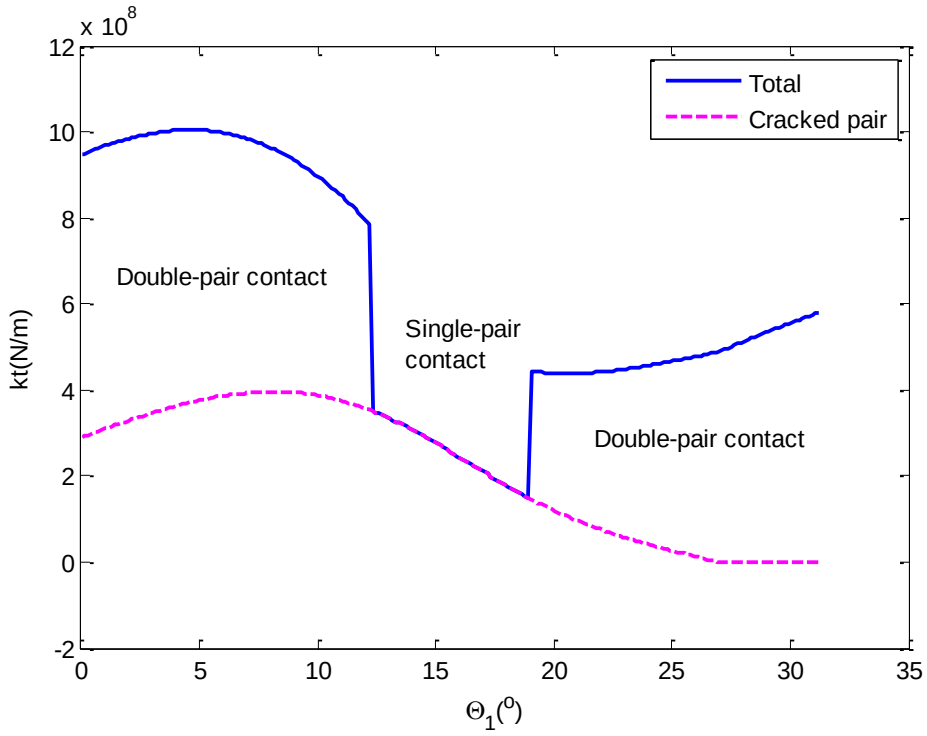

Fig. 6. Mesh stiffness of gears with cracked pinion

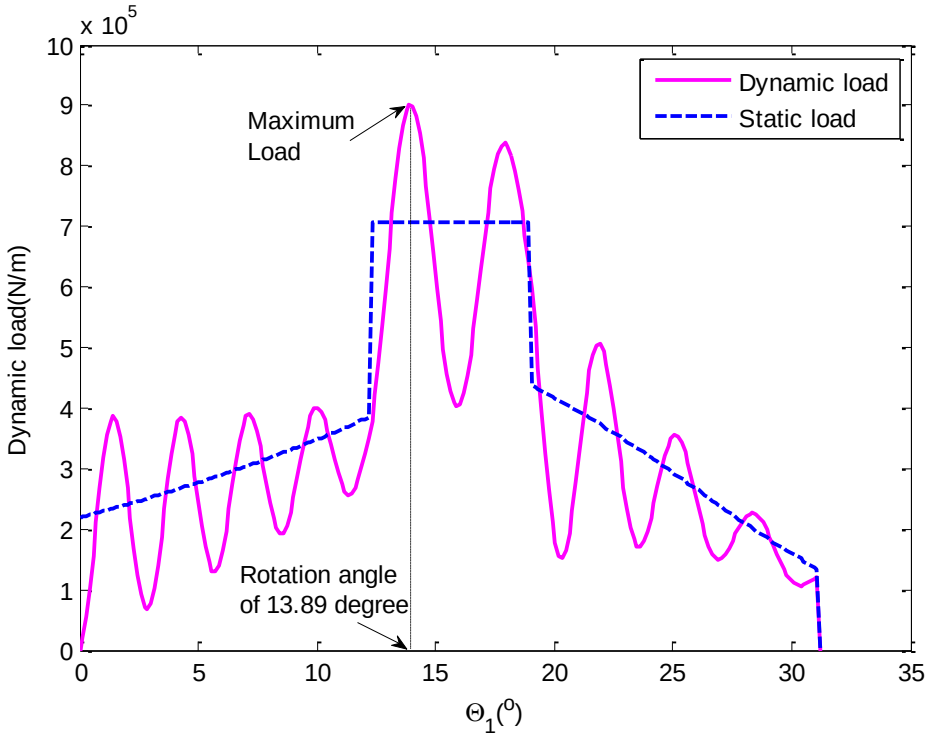

Fig. 7. Dynamic load of pinion with crack of 3.5 mm

The procedure to obtain the history of stress intensity factor as the crack grows to the critical length under varying dynamic load is summarized below:

1. Select initial crack tip T_j, $j = 0$ such that the angle of $\beta_0 = 45$ degree and initial crack length a_0=0.1mm.
2. Calculate u_j which is the distance between tooth root S and T_jG_j. The total mesh stiffness k_t is then obtained by formulas proposed in Section 3.2.2 depending on where the crack tip is and how much degree the rotation angle is.
3. Gear dynamic equations are solved by plugging k_t in MATLAB and the dynamic load is computed using Eqs. (22—23).
4. Apply the maximum load at the contact point on finite element model of cracked pinion tooth which corresponds to the rotation angle of around 14 degree in FRANC2D. The modes I and II stress intensity factors as well as the crack propagation angle are calculated.
5. Propagate crack in that calculated direction with increment of Δa=0.1mm.
6. $j = j + 1$, return to step 2 until the crack length reaches critical value.

Following the procedure above, the history of two modes of stress intensity factors is calculated and shown in Fig. 8. The mode I stress intensity factor K_I is dominant just as stated in other published literatures. So in the Paris' law, only ΔK_I is used to calculate crack propagation rate. The third order polynomial is used to fit the discrete values of K_I obtained by FRANC2D, thus $K_I(a)$ has its continuous form and the value of K_I at each crack length is available. Additionally, since the minimum load during the cracked tooth mesh period is zero, the range of stress intensity factor is just the one obtained under the maximum load. Fig. 9 plots the maximum dynamic load at different crack lengths. Taking maximum dynamic load as the load to apply on the cracked tooth produces larger stress intensity factor compared to static load and under this circumstance, the crack bears a faster propagation rate, which will lead to a relatively shorter remaining useful life.

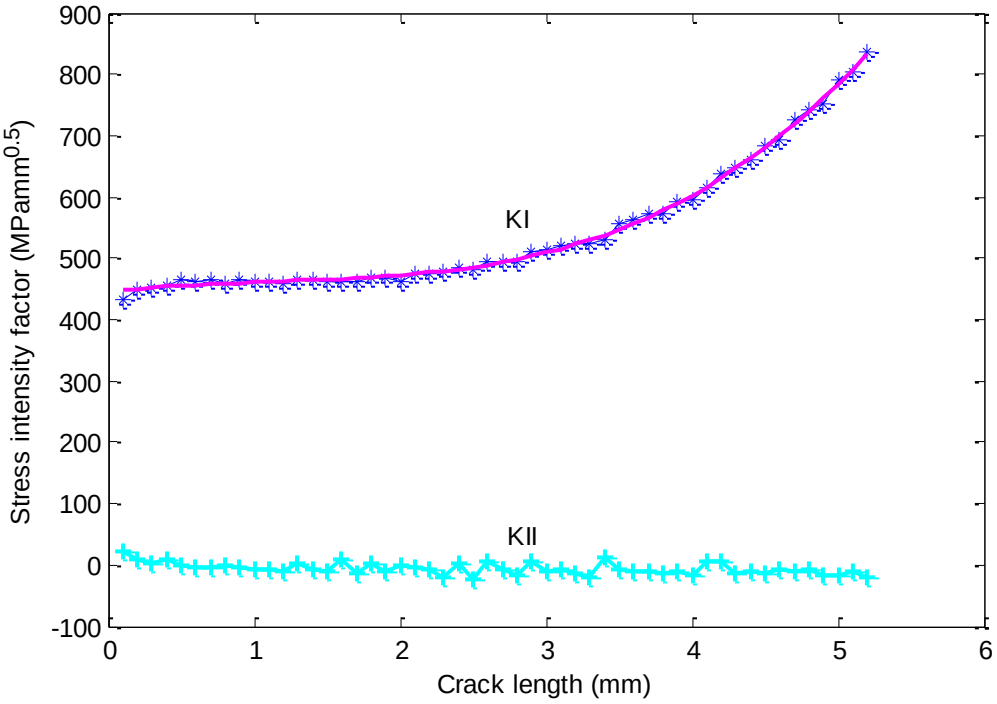

Fig. 8 Stress intensity factor as a function of crack length

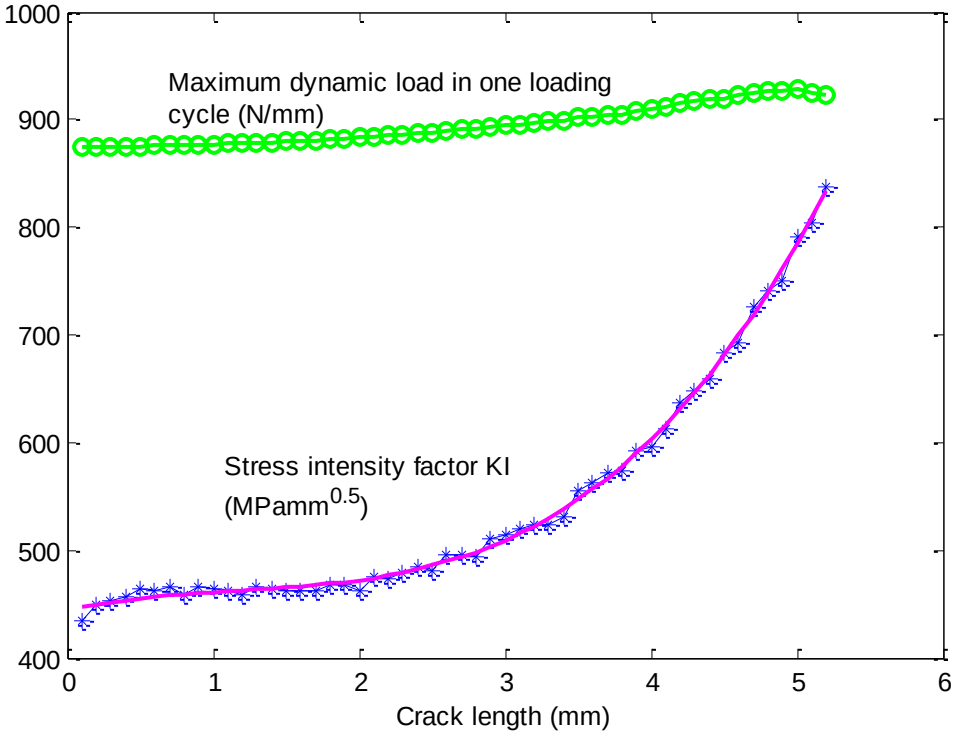

Fig.9 Type I stress intensity factor and maximum dynamic load

To validate the proposed integrated approach, a set of crack degradation paths $\mathcal{P}$ is generated using Paris' law in Eq. (58).

$$\begin{gathered} a\big((i+1)\Delta N\big) = a(i\Delta N) + (\Delta N)C\big[\Delta K\big(a(i\Delta N)\big)\big]^m \varepsilon, i = 0,1,2,\cdots,\lambda-1 \\ a_{mea}(\lambda\Delta N) = a(\lambda\Delta N) + e \\ a(0) = 0.1 \end{gathered} \tag{58}$$

where $\lambda\Delta N$ is the inspection interval. The history of a_{mea} is the generated crack growth path which provides the measured crack length at every inspection cycle. In each degradation path i, parameter m^i is a random sample from its population distribution N_1, and this value is fixed until the critical crack length is reached. Model error ε samples from its normal distribution in each propagation step. And at inspection cycle, measured crack length is generated by adding a random value of measurement error e. All these paths as well as the values of parameter m^i in these paths, termed here as *real* m^i, are recorded. The paths in $\mathcal{P}$ are divided into two sets: training set (H) and test set (R). The training set is used to obtain a prior distribution for parameter m and the test set is used to validate the proposed approach.

To generate the degradation paths, we assume the following values and distributions for the parameters involved:

$$C = 9.12e-11$$

$$\tau = 0.2$$

$$m \sim N(1.4354, 0.2^2)$$

$$\varepsilon \sim N(2.5, 0.5^2)$$

Note that here the uncertainty regarding to m is related to the distribution of the gear population, not of the specific gear being monitored. In this example, 10 degradation paths are generated according to Eq. (58) until the critical crack length a_c =5.2mm, as shown in Fig. 10. Select $\#(H) = 7, \#(R) = 3$. Three test paths #4, #6 and #9 are bolded in Fig. 10. Then for each path $i \in H$, the optimal $m_{op}^i, i = 1,2,\cdots,7$ satisfying the Eq. (56) can be found using optimization. After these seven values of m^i are obtained, termed here as *trained* m^i, normal distribution is used to fit them to obtain a prior for m.

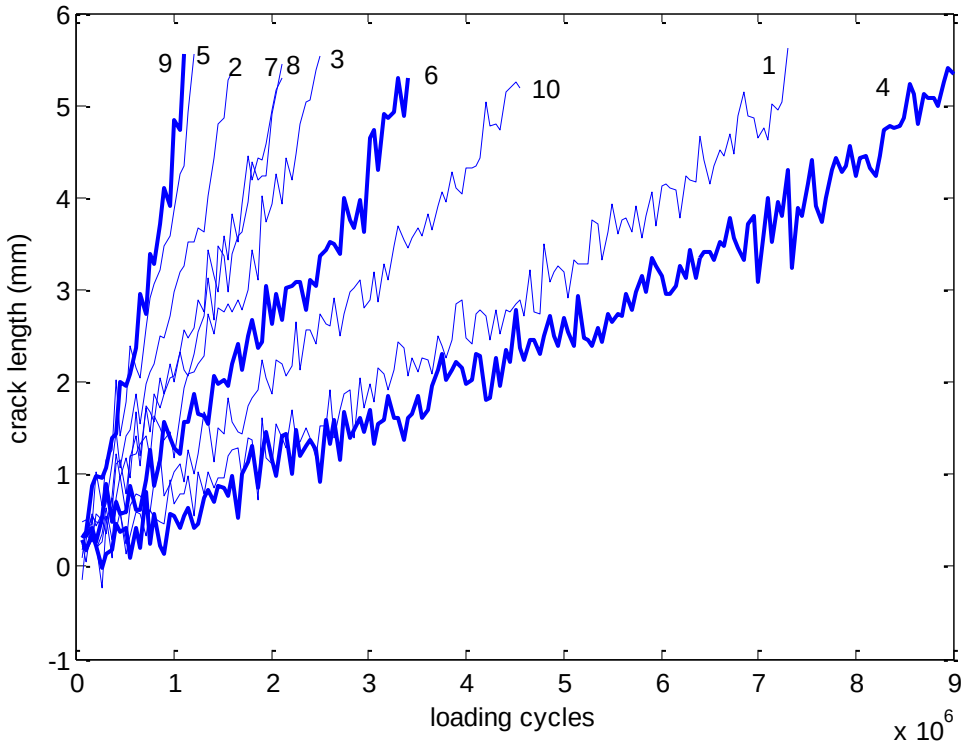

Fig. 10. Ten degradation paths generated using prescribed parameters

4.2 Results

Table 2 shows the ten real values of m for generating these ten paths and the seven trained values for the first seven paths. Then normal distribution is used to fit them. Finally, the prior distribution for m is:

$$f_{prior}(m) \sim N(1.454, 0.1004^2)$$

To validate the proposed prognostics approach, we take paths #4, #6 and #9 for testing. At each cycle for updating, the posterior distribution of m will be the prior distribution for next updating time. In path #4, totally 9×10^6 cycles are consumed to reach the critical length. The updating history for path #4 is shown in Table 3.

In path #6, the failure time is 3.4×10^6 cycles and path #9, totally 1.1×10^6 cycles are consumed. The updating histories for distributions of parameter m in path #6 and path #9 are shown in Table 4 and Table 5, respectively.

Table 2. The real values and the trained values of m

Path #	Real m	Trained m
1	1.2836	1.284
2	1.5302	1.5328
3	1.4569	1.4589
4	1.2495	-
5	1.5724	1.5729
6	1.407	-
7	1.4823	1.4807
8	1.4844	1.4904
9	1.5897	-
10	1.3585	1.3583

Table 3. Test for path #4 to validate proposed approach (real m=1.2495)

Inspection cycle	Crack length (mm)	Mean of m	Std of m
0	0.1	1.454	0.1004
2×10^6	1.1656	1.2746	0.027
4×10^6	1.9857	1.2514	0.0194
6×10^6	3.1521	1.2556	0.016
8×10^6	4.2336	1.2445	0.0121

Table 4. Test for path #6 to validate proposed approach (real m=1.4082)

Cycles when updating m	Crack length (mm)	Mean of m	Std of m
0	0.1	1.454	0.1004
0.7×10^6	0.9349	1.3956	0.037
1.4×10^6	2.0607	1.4194	0.0253
2.1×10^6	2.68	1.3931	0.0186
2.8×10^6	3.7607	1.3967	0.0156

Table 5. Test for path #9 to validate proposed approach (real m=1.59)

Cycles when updating m	Crack length (mm)	Mean of m	Std of m
0	0.1	1.454	0.1004
0.25×10^6	0.9629	1.5409	0.0458
0.5×10^6	1.9648	1.5675	0.0298
0.75×10^6	3.3989	1.6053	0.0201
1×10^6	4.8369	1.5849	0.0111

Table 3, 4 and 5 show that the Bayesian updates adjusted the mean value of m from the initial value 1.454 to its real values gradually, as the condition monitoring data on the crack length are available. Because the RUL is very sensitive to value of m, the distribution adjustment for m is critical for maintenance optimization. Moreover, the standard deviation of m is reduced, which means that the uncertainty in m is reduced through Bayesian updating given the measured crack length. To demonstrate this, Fig.11 shows the updated distribution of m for path #4. The failure time prediction results for path #4, #6 and #9 are shown in Fig. 12, 14 and 15 respectively, from which we can see, with the updates for distribution of m at certain inspection cycles, the prediction of failure time distribution becomes narrower and the mean is approaching the real failure time. The updated RUL at each inspection cycle for path #4 is also computed shown in Fig. 13 and the vertical lines represent the real RUL at those inspection cycles.

5. Conclusions

Accurate health prognosis is critical for ensuring equipment reliability and reducing the overall life-cycle costs, by taking full advantage of the useful life of the equipment. In this paper, we develop an integrated prognostics method for gear remaining life prediction, which utilizes both gear physical models and real-time condition monitoring data. In the developed integrated prognostics method, we have specifically developed the general prognosis framework for gears, a gear FE model for gear stress analysis, a gear dynamics model for dynamic load calculation, and a damage propagation model described using Paris' law. A gear mesh stiffness computation

method is developed based on the gear system potential energy, which results in more realistic curved crack propagation paths. Material uncertainty and model uncertainty factors are considered to account for the differences among different specific units that affect the damage propagation path. A Bayesian method is used to fuse the collected condition monitoring data to update the distributions of the uncertainty factors for the current specific unit being monitored, and to achieve the updated remaining useful life prediction.

Example based on simulated degradation data are used to demonstrate the effectiveness of the proposed approach. The results demonstrate that the proposed integrated prognostics method can effectively adjust the model parameters based on the observed degradation data, and thus lead to more accurate remaining useful life predictions, and the prediction uncertainty can be reduced with the availability of condition monitoring data.

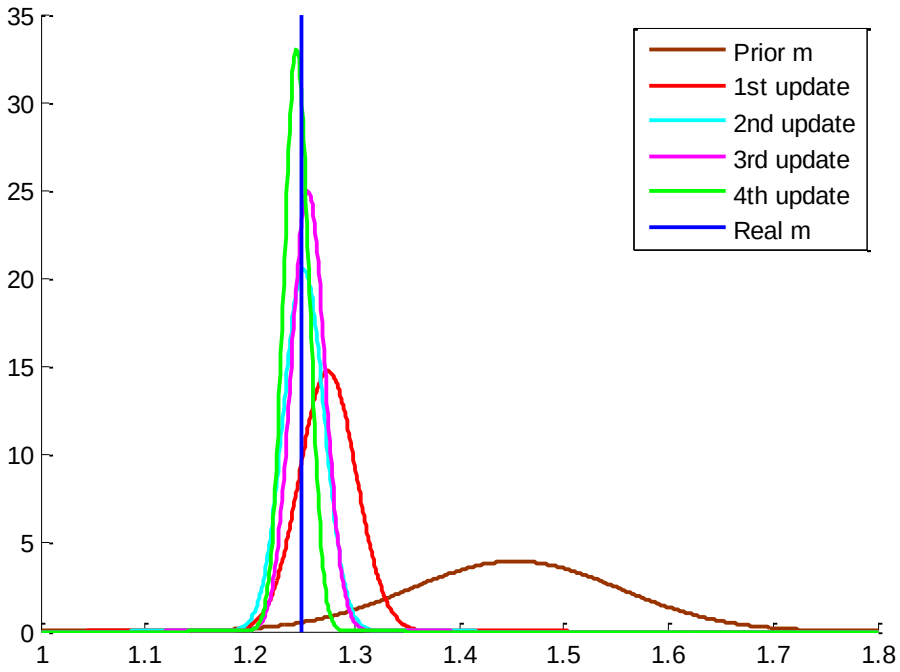

Fig. 11. Updated distributions of m

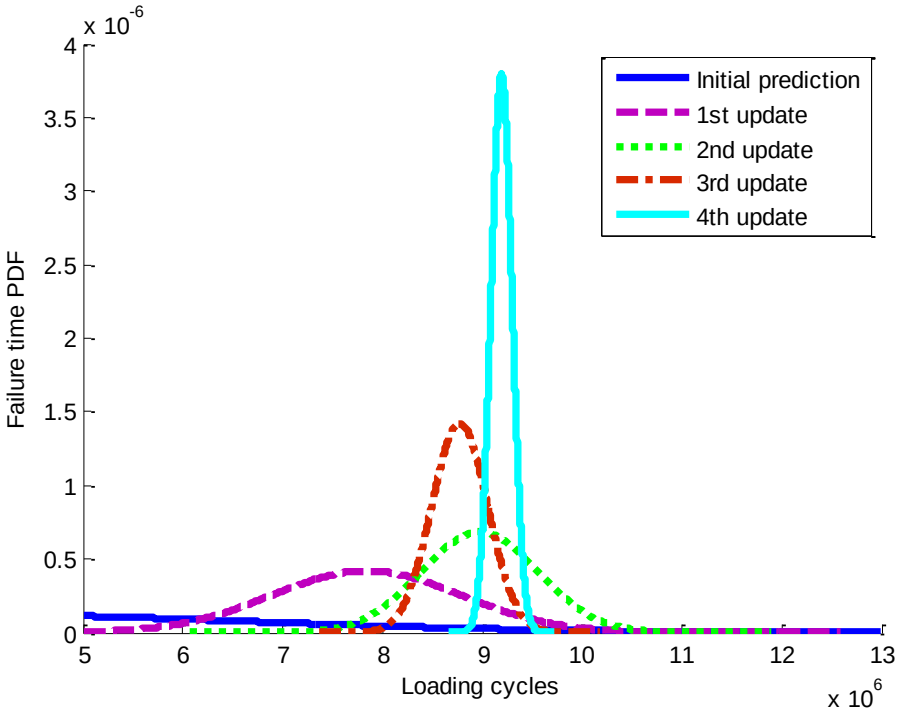

Fig. 12. Updated failure time distribution for path #4

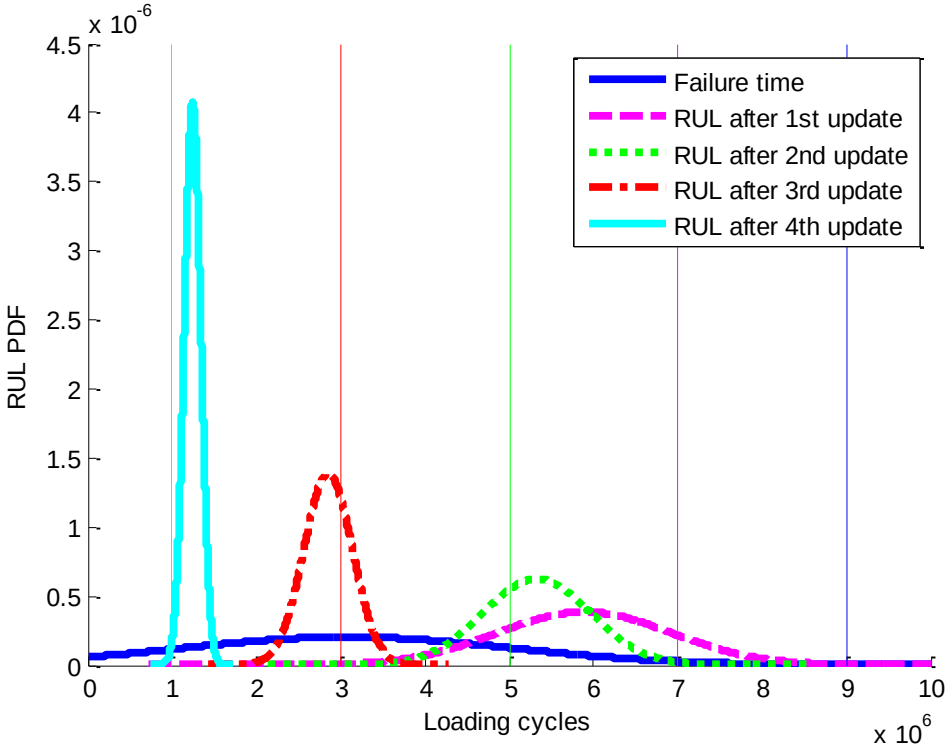

Fig. 13. Updated RUL for path #4

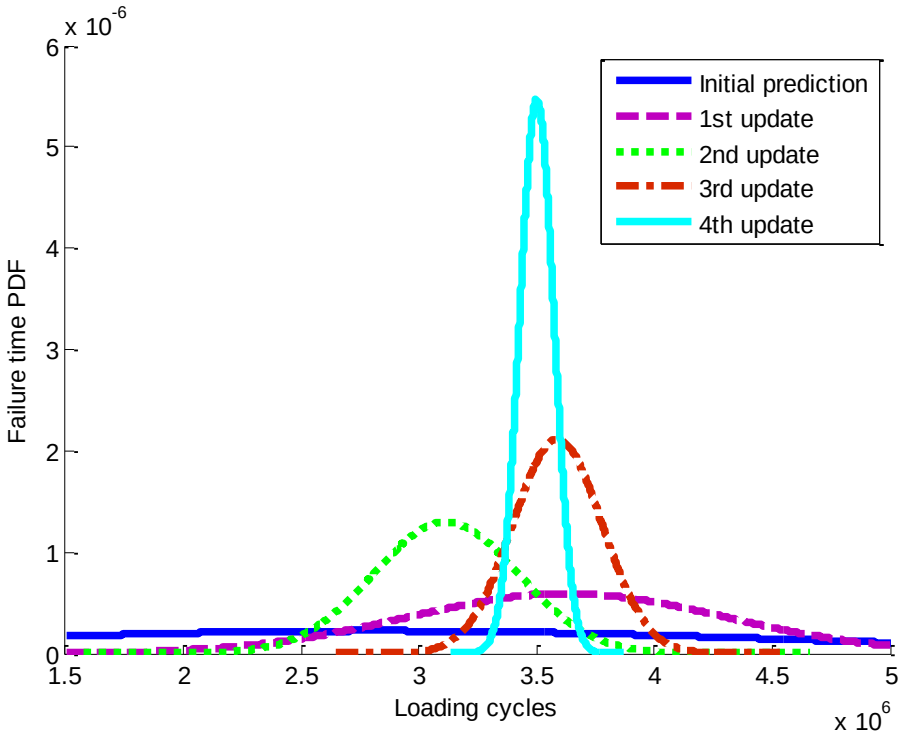

Fig. 14. Updated failure time distribution for path #6

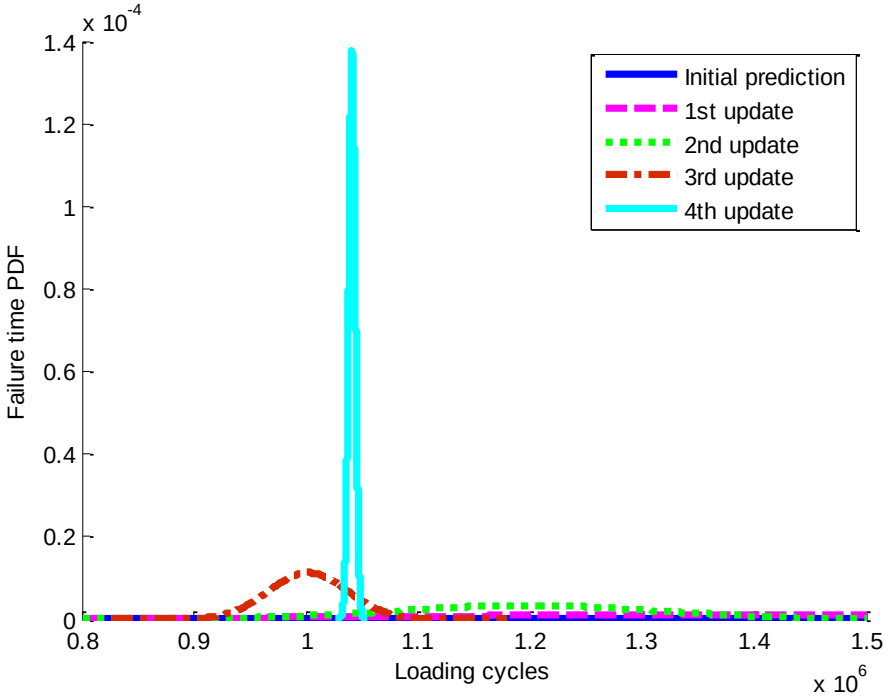

Fig. 15. Updated failure time distribution for path #9

Acknowledgments

This research is supported by Le Fonds québécois de la recherche sur la nature et les technologies (FQRNT) and the Natural Sciences and Engineering Research Council of Canada (NSERC).

References

[1]. A.K.S. Jardine, D.M. Lin, and D. Banjevic, "A review on machinery diagnostics and prognostics implementing condition-based maintenance", *Mechanical Systems and Signal Processing*, vol. 20, no.7, pp. 1483-1510, 2006.

[2]. G. Vachtsevanos, F.L. Lewis, M. Roemer, A. Hess, and B. Wu, *Intelligent Fault Diagnosis and Prognosis for Engineering Systems*, John Wiley & Sons, 2006.

[3]. Z. Tian, M.J. Zuo, and S. Wu. "Crack propagation assessment for spur gears using model-based analysis and simulation", *Journal of Intelligent Manufacturing*, Available online from November 2009. doi: 10.1007/s10845-009-0357-8. 2009a

[4]. C.J. Li and H. Lee, "Gear fatigue crack prognosis using embedded model, gear dynamic model and fracture mechanics", *Mechanical Systems and Signal Processing*, vol. 19, no. 4, pp. 836–846, 2005.

[5]. G.J. Kacprzynski, A. Sarlashkar, M.J. Roemer, A. Hess, and G. Hardman. "Predicting remaining life by fusing the physics of failure modeling with diagnostics", *Journal of The Minerals, Metals and Materials Society*, vol. 56, no. 3 pp. 29-35, 2004.

[6]. S. Marble and B.P. Morton, "Predicting the remaining life of propulsion system bearings", in *Proceedings of the 2006 IEEE Aerospace Conference*, Big Sky, MT, USA, 2006.

[7]. D. Banjevic, A.K.S. Jardine, and V. Makis V, "A control-limit policy and software for condition-based maintenance optimization", *INFOR*, vol. 39, no. 1, pp. 32–50, 2001.

[8]. N. Gebraeel, M.A. Lawley, and R. Liu, "Residual life, predictions from vibration-based degradation signals: A neural network approach", *IEEE Transactions on Industrial*

Electronics, vol. 51, no. 3, pp. 694-700, 2004.

[9]. N. Gebraeel and M.A. Lawley, "A neural network degradation model for computing and updating residual life distributions", *IEEE Transactions on Automation Science And Engineering*, vol. 5, no. 1, pp. 154-163, 2008.

[10]. J. Lee, J. Ni, D. Djurdjanovic, H. Qiu and H. Liao, "Intelligent prognostics tools and e-maintenance", *Computers in Industry*, vol. 57, no. 6, pp. 476-489, 2006.

[11]. Z. Tian, L. Wong, and N. Safaei. "A neural network approach for remaining useful life prediction utilizing both failure and suspension histories", *Mechanical Systems and Signal Processing*, vol. 24, no. 5, pp. 1542-1555, 2010.

[12]. Z. Tian and M.J. Zuo. "Health condition prediction of gears using a recurrent neural network approach", *IEEE Transactions on Reliability*, vol. 59, no. 4, pp. 700-705, 2010.

[13]. N. Gebraeel, M. Lawley, R. Li, and J.K. Ryan, "Life Distributions from Component Degradation Signals: A Bayesian Approach", *IIE Transactions on Quality and Reliability Engineering*, vol. 37, no. 6, pp. 543-557, 2005.

[14]. H. Liao, and Z. Tian, "A general framework for remaining useful life prediction for a single unit under time-varying operating conditions", *IIE Transactions*, Under review, 2011.

[15]. A. Coppe, R.T. Haftka, and N.H. Kim, "Uncertainty reduction of damage growth properties using structural health monitoring", *Journal of Aircraft*, vol. 47, no. 6, pp. 2030-2038, 2010.

[16]. P. C. Paris and F. Erdogen, "A critical analysis of crack propagation laws", *Journal of Basic Engineering*, vol. 85, no. 4, pp. 528-534, 1963

[17]. J. E. Collipriest, "An experimentalist's view of the surface flaw problem", *The Surface Crack: Physical Problems and Computational Solutions, American Society of Mechanical Engineers*, pp. 43-61, 1972

[18]. K. Inoue, M. Kato, G. Deng, and N. Takatsu, "Fracture mechanics based of strength of carburized gear teeth", in *Proceedings of the JSME International Conference on Motion and Power Transmissions*, Hiroshima, Japan, 1999, pp. 801-806

[19]. S. Zouari, M. Maatar, T. Fakhfakh, and M. Haddar, "Following spur gear crack propagation in the tooth foot by finite element method", *Journal of Failure Analysis and Prevention*, vol. 10, no. 6, pp. 531-539, 2010

[20]. S. Glodez, M. Sraml, and J. Kramberger, "A computational model for determination of

service life of gears", *International Journal of Fatigue*, vol. 24, no. 10, pp. 1013-1020, 2002

[21]. W. Bartelmus. "Mathematical modelling and computer simulations as an aid to gearbox diagnostics", *Mechanical Systems and Signal Processing*, vol. 15, no. 5, pp. 855–871, 2001.

[22]. H-H. Lin, R. L. Huston, and J. J. Coy, "On dynamic loads in parallel shaft transmissions: part I - modeling and analysis", Journal *of Mechanisms, Transmissions, and Automation in Design*, vol. 110, no. 2, pp. 221-225, 1988

[23]. D. G. Lewicki, R. F. Handschuh, L. E. Spievak, P. A. Wawrzynek, and A. R. Ingraffea, "Consideration of moving tooth load in gear crack propagation predictions", *Journal of Mechanical Design*, vol. 123, no. 1, pp. 118-124, 2001

[24]. D. C. H. Yang and J. Y. Lin, "Hertzian damping, tooth friction and bending elasticity in gear impact dynamics", *Journal of Mechanisms, Transmissions, and Automation in Design*, vol. 109, pp. 189-196, 1987

[25]. X. H. Tian, M. J. Zuo and K. R. Fyfe, "Analysis of the vibration response of a gearbox with gear tooth faults", in *Proceedings of IMECE04, 2004 ASME International Mechanical Engineering Congress and Exposition*, Anaheim, CA, USA, 2004

[26]. S. Wu, M. J. Zuo and A. Parey, "Simulation of spur gear dynamics and estimation of fault growth", *Journal of Sound and Vibration*, vol. 317, pp. 608-624, 2008

[27]. D. An, J. Choi, and N.H. Kim, "Identification of correlated damage parameters under noise and bias using Bayesian inference", *Structural Health Monitoring*, vol. 11, no. 3, pp. 293-303, 2012

[28]. M. E. Orchard and G. J. Vachtsevanos, "A particle filtering approach for on-line failure prognosis in a planetary carrier plate", *International Journal of Fuzzy Logic and Intelligent Systems*, vol. 7, no. 4, pp. 221-227, 2007

[29]. M. E. Orchard and G. J. Vachtsevanos, "A paricle filtering-based framework for real-time fault diagnosis and failure prognosis in a turbine engine", *2007 Mediterranean Conference on Control and Automation*, Athens, Greece, 2007

[30]. S. Sankararaman, Y. Ling and S. Mahadevan, "Confidence assessment in fatigue damage prognosis", *Annual Conference of the Prognostics and Health Management Society*, Portland, Oregon, 2010

Biographies

Fuqiong Zhao is currently a Ph.D. candidate in the Department of Mechanical and Industrial Engineering at Concordia University, Canada. She received her M.S. degree in 2009 and B.S. degree in 2006 both from the School of Mathematics and System Sciences, Shandong University, China. Her research is focused on integrated prognostics, uncertainty quantification, finite element modeling and condition monitoring.

Zhigang Tian is currently an Associate Professor in the Concordia Institute for Information Systems Engineering at Concordia University, Canada. He received his Ph.D. degree in 2007 in Mechanical Engineering at the University of Alberta, Canada, and his M.S. degree in 2003 and B.S. degree in 2000 both in Mechanical Engineering at Dalian University of Technology, China. His research interests focus on reliability analysis and optimization, condition monitoring, prognostics, maintenance optimization and renewable energy systems. He is a member of IIE and INFORMS.

Yong Zeng is a Professor in the Concordia Institute for Information Systems Engineering at Concordia University, Montreal, Canada. He is Canada Research Chair in Design Science (2004–2014). He received his B.Eng. degree in structural engineering from the Institute of Logistical Engineering and M.Sc. and Ph.D. degrees in computational mechanics from Dalian University of Technology in 1986, 1989, and 1992, respectively. He received his second Ph.D. degree in design engineering from the University of Calgary in 2001. His research is focused on the modeling and computer support of creative design activities.